Note: This file was corrected on 10 May 2005, see page 4.

Science Supporting Online Material

Attractor Dynamics in the Hippocampal Representation of the Local Environment

Tom J. Wills,[1] Colin Lever,[1] Francesca Cacucci,[1] Neil Burgess,[1,2] John O'Keefe[1]*

[1]Department of Anatomy and Developmental Biology, and [2]Institute of Cognitive Neuroscience, University College London, London, WC1E 6BT, UK.

MATERIALS AND METHODS

Animals

Six Lister Hooded rats maintained on a 12:12 hour light:dark (lights off: 3 p.m.) schedule, weighing 280–380 g at time of surgery, were used as subjects.

Testing procedures

Experiments were conducted in a black-curtained, circular testing arena 2.5-m diameter. Rats were kept on a holding platform outside the arena before and after every trial. Testing environments were placed on a circular black platform 90 cm in diameter, which was cleaned before every trial. The centre of each testing environment had the same location relative to the curtained arena. An external white cue card (102 cm wide, 77 cm high) and standardized procedures for placing the rat into the box provided directional constancy throughout all trials. During trials the rat searched for grains of sweetened rice randomly thrown into the box about every 20 s. Two testing enclosures were used: a 'morph' box and a white wooden circle. The morph box (*S1*) is made from 32 pieces of rectangular cross-section plastic tubing, 7.5 cm wide, 50 cm high, held together on the inner surface by brown packing tape, covered with masking tape. It can be configured as a 79 cm diameter circle, a 62 cm sided square, and various octagons (see Fig. S1, a-d, for more details). The wooden circle measured 79 cm diameter, 50 cm high, with a smooth, painted, white inner surface. All trials were 10 minutes in duration, with 20 minute inter-trial intervals. Rats were trained with six trials per day: days 1-3, alternating morph square and white wooden circle; day 4, alternating square and circle, 2nd trial: white circle, 4th and 6th trial: morph circle; days 5-6: alternating morph square and morph circle. Octagon probe series was presented on day 7. (See Fig. S1, c and e, for details).
Cell recording

Methods of extracellular tetrode recording and analysis were as previously reported (*S1*, *S2*). Electrodes were moved into the CA1 pyramidal cell layer while rats sat on a holding platform in a different room. First exposure to the test environments occurred only after stable recording had been achieved, 2 to 4 weeks following surgery. Place units were isolated offline. Firing-rate maps were constructed by finding the number of spikes and the rat's dwell time in each 2 cm sided location bin, smoothing using a boxcar average over the 5 × 5 surrounding bins, and dividing the number of spikes by dwell time. They are shown as colour plots with each colour autoscaled to represent 20% of the peak rate (red to dark blue). Unvisited bins are shown in white. As previously (*S1*, *S2*), trials in which the firing rate fails to exceed 1.0 Hz are deemed not to express a spatial field and are shown as dark blue.

Data analysis

For comparison of firing rate maps from trials in different shaped boxes, corresponding bins in the different shapes were defined as those with the same direction from the centre and proportion of distance from the centre to the edge along that direction [a transformation that preserves the similarity of un-remapped fields (*S1*)], using nearest neighbour interpolation. Remapping was assessed using Pearson's *r* correlation over corresponding pairs of visited bins, excluding those with 0 Hz firing rate in both trials. A cell was considered stably *remapped* if the mean Square-Circle correlation was 0.5 less than the mean Square-Square and Circle-Circle correlation, i.e.:

$$\langle r\rangle_{SC} < \tfrac{1}{2}(\langle r\rangle_{SS} + \langle r\rangle_{CC}) - 0.5$$

where $\langle\rangle_{SS}$ indicates the average over all pairs of trials in Square boxes, $\langle\rangle_{CC}$ average over pairs of Circle trials, and $\langle\rangle_{SC}$ average over pairs of trials, one in each shape. Stable remapping over the 3 Square and Circle baselines (which span the probe trials-see below) is important to prevent temporal instability being confounded with effects of probe shape.

For remapped cells, the similarity of the firing pattern in a given shape I to that in the 3 Square baseline trials, relative to its similarity to that in the 3 Circle baseline trials, is defined as:

$$s(\mathrm{I}, \mathrm{S}) = (\langle r\rangle_{IS} - \langle r\rangle_{SC})/(\langle r\rangle_{SS} - \langle r\rangle_{SC})$$

where $\langle\rangle_{IS}$ is the average over pairs of trials, one in shape I and one in the Square. A value of 1.0 indicates a firing pattern identical to that in the Square, a value of 0.0 indicates firing as different to that in the Square as the firing in the Circle is. Similarly, we define the similarity of firing in shape I to that in the Circle, relative to that in the Square as:

$$s(\mathrm{I}, \mathrm{C}) = (\langle r\rangle_{IC} - \langle r\rangle_{SC})/(\langle r\rangle_{CC} - \langle r\rangle_{SC}).$$

Both similarity measures are necessary, because lack of similarity to the Square does not necessarily imply similarity to the Circle, and vice versa. These measures work well when a field is expressed in both shapes, or in one shape but not the other, but they do not reliably reflect similarity in pairs of low-rate shapes (i.e., both < 1.0Hz). In this case we replace correlation coefficients with peak-rate similarity:

$$R(\mathrm{A},\mathrm{B}) = \min(\text{peak rate A, peak rate B})/\text{mean}(\text{peak rate A, peak rate B})$$

(this measure behaves similarly to *r* for rate-remapped cells for trials with > 1 Hz peak rate, is more stable for trials with < 1Hz peak rates, but does not capture field position remapping), so that the similarity to Square measure becomes:

$$s(\mathrm{I}, \mathrm{S}) = (\langle R\rangle_{IS} - \langle R\rangle_{SC})/(\langle R\rangle_{SS} - \langle R\rangle_{SC})$$

and likewise for similarity to Circle.

For analysis of 10-s intervals (Fig. 4, A and B), the similarity measure is applied as above, using the firing rate map derived from the 10-s interval for trial I and the full duration rate maps for baseline trials S and C (two 10-s interval maps do not contain sufficient pairs of mutually visited bins for meaningful correlations), and the correlation *r* is used in all cases (peak-rate similarity *R* cannot be used as the animal does not adequately sample the environment in 10-s, often missing the centre of the place field).

Cells that fired no spikes in the given intervals for a given shape are omitted from the similarity data for that interval and shape. Note that the similarity of a 10-s interval in the Square to Square baselines is less than 1.0 (and its similarity to Circle baselines less than 0.0) due to the greater noise in these maps than in full duration maps. Linear regression was performed on the difference in similarity to square and circle baselines, i.e.: s(I, S) - s(I, C), of the individual cells.

Note: This file was corrected on 10 May 2005 to change lights on to lights off at 3 p.m. in the first line of text and to correct two equations within the legend to Fig. 3. The originally posted version is available here.

SUPPORTING FIGURE 1

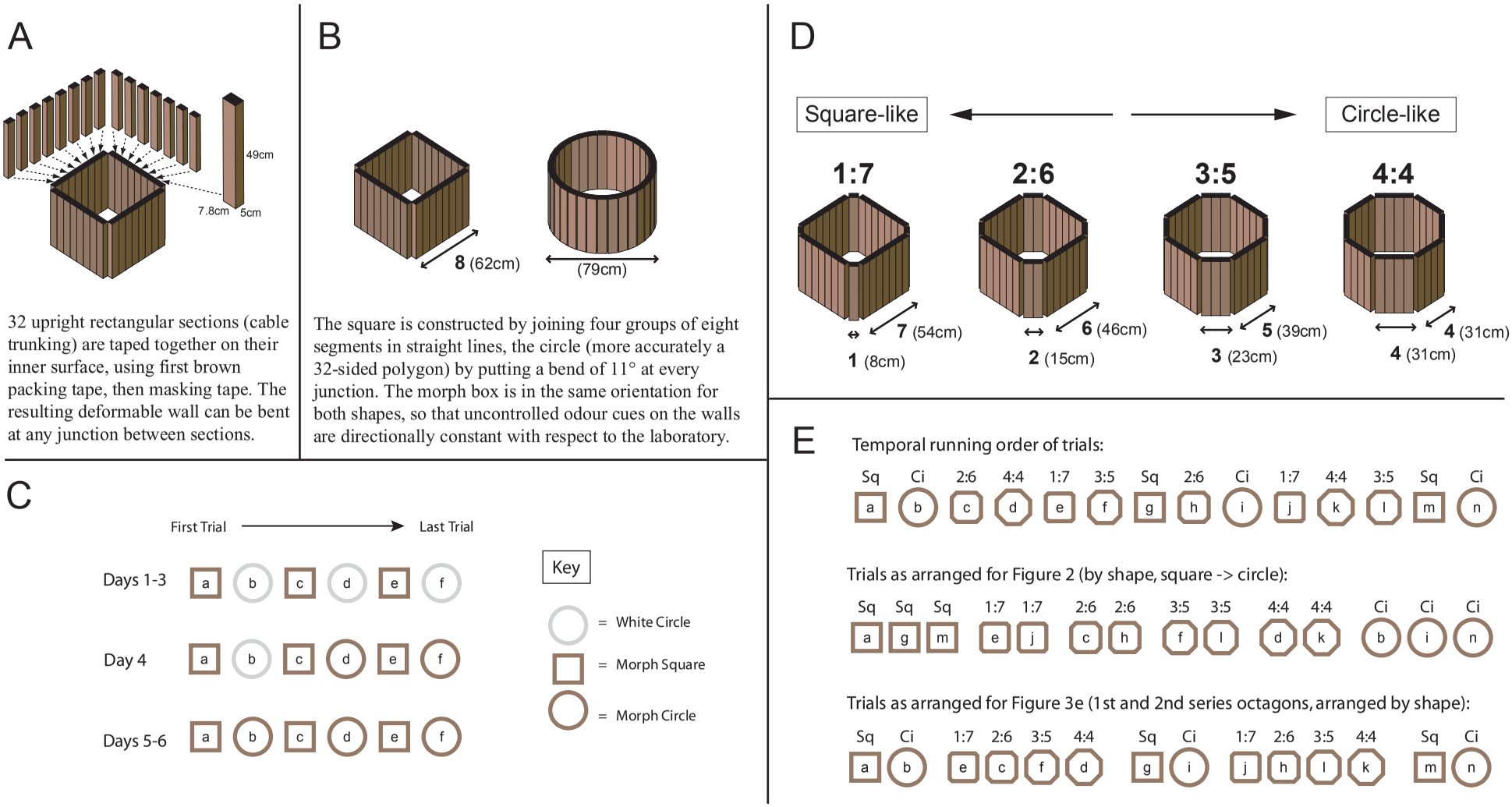

Fig. S1. Methods for Rapid Remapping and Octagon Probe experiments. A) Construction of morph box. B) Morph box configured as square and circle. C) Protocol for rapid remapping training. Colour of outline shapes indicate type of material, see key for details. Letters inside shapes indicate temporal order of trials. All trials 10 mins, inter-trial interval 20 mins. D) Morph box configured as intermediate octagons, for octagon probe trials. Octagons incrementally intermediate between square and circle are constructed by changing the relative lengths of adjacent sides. All internal angles are always 135°. These shapes are labelled according to the number of morph box sections that make up the adjacent sides. E) Protocol for Octagon Probe Trials. Top row: trials in actual running order. Letters inside shape indicate temporal order of trials. All environments constructed using morph box. All trials 10 mins, inter-trial interval 20 mins. Middle and bottom rows: order of trials rearranged to match presentation in figures 2 (middle), 3E (bottom).

SUPPORTING FIGURE 2

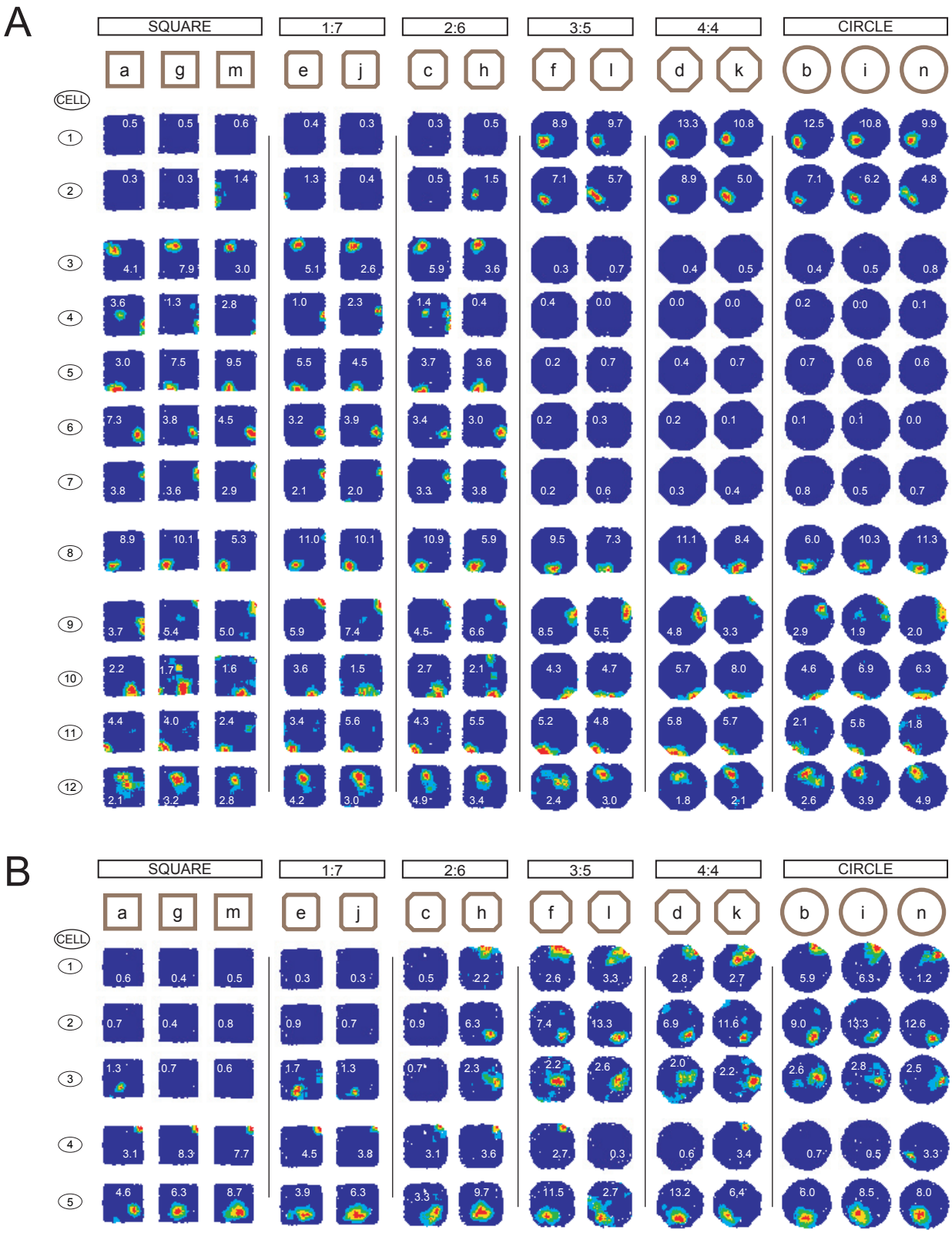

Fig. S2. Abrupt and coherent remapping between square-like and circle-like representations during intermediate octagonal environments. Layout of maps as for fig. 2. (A) Rat 1. Cells 1-8 switch from square-like to circle-like representations between 2:6 and 3:5 octagons on both 1st and 2nd series. Cells 9-12 did not reach our criterion for remapping. (B) Rat 3. Cells 1-3 switch representations between 2:6 and 3:5 octagons on the first series, and between 1:7 and 2:6 octagons on the second series. Cells 4-5 did not reach our criterion for remapping. See Materials and Methods for details.

SUPPORTING FIGURE 3

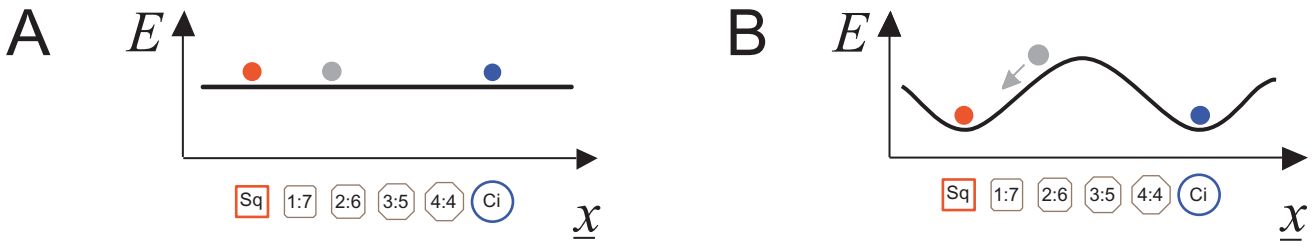

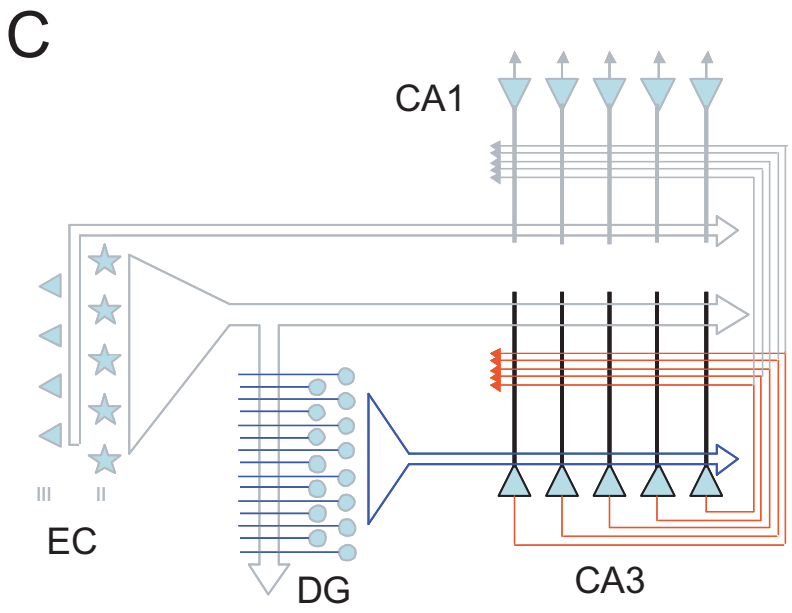

Fig. S3. (A) Continuous representations x (vector of activity of N place cells) in the absence of attractors. The place cell representation of an environment of intermediate shape (grey point) is intermediate to those for the square or circular environments (x^S and x^C, red and blue points respectively), consistent with a feed forward transformation of environmental inputs (*S2,S3*). (B) Attractor representations of square and circular environments (x^S and x^C) after fast remapping. The place cell representation of an environment of intermediate shape (x, grey point) falls into the basin of attraction of the circular or square representation and converges onto that representation over time (grey arrow). This behaviour could result from modification of recurrent connections between place cells. In one of the simplest models (*S4*), activity of cell i is modelled as $x_i = \pm 1$. Connections between cells i and j are symmetric, with synaptic 'weight' $w_{ij} = w_{ij}$. The dynamics of the system are given by: $x_i(t+1) = \text{sign}(\Sigma_j w_{ij} x_j(t))$, such that the 'energy' or Lyapunov function of the system: $E \propto -\Sigma_{ij} w_{ij} x_i x_j$, can only reduce. If connection weights undergo a form of Hebbian learning during representations x^S and x^C (such that $w_{ij} \propto \Sigma_{\mu=S,C} x_i^\mu x_j^\mu$) then these representations become attractors: similar enough representations to x^S or x^C converge onto that representation. Similar behaviour is also shown by more biologically realistic models (*S5-S8*). (C) Postulated functional anatomy of the hippocampus (*S6,S7,S9-S13*). The pathway from entorhinal cortex (EC) to CA3 drives the place cell representation. Remapping (blue connections): The large number of cells in the dentate gyrus (DG) allows pattern separation of the EC input, with plasticity in the EC-DG pathway causing remapping. The powerful and selective DG-CA3 pathway imposes new representations in CA3, with plasticity in the EC-CA3 pathway allowing the EC input to drive the new representation. Attractors (red connections): The dense recurrent connections between CA3 pyramidal cells mediate an attractor or auto-associative network in CA3: plasticity in these connections allows a representation to become an attractor. The attractor-mediated CA3 representation drives the CA1 representation via the CA3-CA1 pathway, and could be compared to the EC representation via the projection from small pyramidal cells in EC layer III.

References and Notes

S1. C. Lever, T. Wills, F. Cacucci, N. Burgess, J. O'Keefe, *Nature* **416**, 90 (2002).

S2. J. O'Keefe and N. Burgess, *Nature* **381**, 425 (1996).

S3. T. Hartley, N. Burgess, C. Lever, F. Cacucci, J. O'Keefe, *Hippocampus* **10**, 369 (2000).

S4. J. J. Hopfield, *Proc.Natl.Acad.Sci.U.S.A* **79**, 2554 (1982).

S5. D. J. Amit, *Modelling Brain Function: The World of Attractor Neural Networks* (Cambridge University Press, Cambridge, 1992).

S6. A. Treves and E. T. Rolls, *Hippocampus* **2**, 189 (1992).

S7. J. L. McClelland, B. L. McNaughton, R. C. O'Reilly, *Psychol.Rev.* **102**, 419 (1995).

S8. A. Samsonovich and B. L. McNaughton, *J. Neurosci.* **17**, 5900 (1997).

S9. D. Marr, *Philos. Trans. R. Soc. Lond. B Biol. Sci.* **262**, 23 (1971).

S10. B. L. McNaughton and R. G. Morris, *Trends Neurosci.* **10**, 408 (1987).

S11. K. Nakazawa et al., *Science* **297**, 211 (2002).

S12. M. E. Hasselmo, B. P. Wyble, G. V. Wallenstein, *Hippocampus* **6**, 693 (1996).

S13. K. I. Blum and L. F. Abbott, *Neural Comput.* **8**, 85 (1996).